

# Generalized correlated states in a ring of coupled nonlinear oscillators with a local injection

Y. Chembo Kouomou<sup>1,2</sup> and P. Wofo<sup>1,\*</sup>

<sup>1</sup>Laboratoire de Mécanique, Faculté des Sciences, Université de Yaoundé I, Boîte Postale 812, Yaoundé, Cameroon

<sup>2</sup>Division of Telecommunication Technical Studies, Minpostel, Yaoundé, Cameroon

(Received 18 July 2002; published 4 December 2002)

In this paper, we study the spatiotemporal dynamics of a ring of diffusely coupled nonlinear oscillators. Floquet theory is used to investigate the various dynamical states of the ring, as well as the Hopf bifurcations between them. A local injection scheme is applied to synchronize the ring with an external master oscillator. The shift-invariance symmetry is thereby broken, leading to the emergence of generalized correlated states. The transition boundaries from these correlated states to spatiotemporal chaos and complete synchronization are also derived. Numerical simulations are performed to support the analytic approach.

DOI: 10.1103/PhysRevE.66.066201

PACS number(s): 05.45.Xt

## I. INTRODUCTION

Synchronization and spatiotemporal dynamics of chaotic systems are some of the most intensively investigated topics of nonlinear science [1–3]. It is known that these phenomena can lead to interesting applications in communication engineering [4] or for the understanding of certain collective behaviors encountered in various physical and biological systems [5,6].

In general, when several identical oscillators are coupled, different dynamical states can be observed such as spatiotemporal chaos or complete synchronization. It has yet been demonstrated that the occurrence of these dynamical states mostly relies on the number of oscillators, as well as on the type and strength of the coupling [7–10]. However, the modeled system or its potential utilization sometimes requires to couple the system to an external independent oscillator. This is commonly achieved through the local injection technique consisting of a unidirectional coupling between the external command oscillator and a fixed representative of the nonlinear coupled system [11]. This local injection scheme is, for example, indispensable for the description of undesirable parasite couplings or external perturbations. On the other hand, local injection can also be willingly introduced to force the nonlinear system to replicate the dynamics of the external master oscillator. For example, it is known that initially chaotic oscillators can lock into a (multi-) periodic state when they are mutually coupled [10]. The local injection method can, in that case, enable to recover the chaotic dynamics when the unidirectional command coupling is suitably designed.

In this paper, we consider a shift-invariant set of  $N$  diffusely coupled single-well Duffing oscillators (SWDOs) with a positive nonlinear stiffness coefficient. Straightforwardly taking into account the injection unidirectional coupling, the evolution equations can be written as

$$\ddot{x}_1 + \lambda \dot{x}_1 + x_1 + \gamma x_1^3 = F \cos \omega t + K(x_2 - 2x_1 + x_N) + G(\bar{x}_c - x_1),$$

$$\ddot{x}_k + \lambda \dot{x}_k + x_k + \gamma x_k^3 = F \cos \omega t + K(x_{k+1} - 2x_k + x_{k-1}),$$

$$k = 2, \dots, N, \quad (1)$$

where  $\bar{x}_c$  represents the dynamics of the external oscillator and plays the role of a command signal,  $x_k$  stands for the instantaneous displacement of the  $k$ th oscillator,  $K$  and  $G$ , respectively, represent the coupling parameter and the local injection strength. The  $N$  state variables  $x_k$  obey to the shift-invariance condition  $x_k \equiv x_{k+N}$ . Generally, literature lays emphasis upon the case  $\bar{x}_c \equiv 0$ , i.e., upon the control of the coupled system to the trivial equilibrium state. Even for this simplest target, further simplifications are often imposed for analytical results to be derived. For example,  $G$  may be directly set to infinity to pin at least the first oscillator to 0, and gradient-coupling forces are sometimes introduced to enhance the control efficiency [11]. Throughout our study we take  $\bar{x}_c$  as the chaotic oscillation of a SWDO identical to the uncoupled items of the ring, i.e., we have

$$\ddot{\bar{x}}_c + \lambda \dot{\bar{x}}_c + \bar{x}_c + \gamma \bar{x}_c^3 = F \cos \omega t. \quad (2)$$

For the sake of exemplification, we fix  $N$  to 4, and we aim to analyze the influence of the local injection on the dynamics of the nonlinear coupled system. More precisely, our objective is first to identify the various dynamical states of the ring depending on  $K$ , and second to study the modifications induced by the local injection coupling.

The paper is organized as follows. In Sec. II, we analyze the dynamics of the nonlinear coupled system when  $G=0$ . The transitions from spatiotemporal chaos to complete synchronization states are particularly investigated through Floquet theory. Section III deals with the case  $G \neq 0$ , and it is demonstrated that the local injection coupling drastically modifies the dynamical behavior of the ring as it enables what we have termed generalized correlated states to emerge. We also give an analytic insight into the nature of these correlated states and discuss their potential applications, mainly in the field of communication engineering. The fourth and last section is devoted to the conclusion.

\*Corresponding author. Email address: pwofo@uycdc.uninet.cm

**II. NONLINEAR DYNAMICS AND BIFURCATION BEHAVIOR OF THE FOUR-OSCILLATOR RING ( $G=0$ )**

The SWDOs with a positive nonlinear stiffness term can display a chaotic dynamics as it appears in Fig. 1 with a pseudo-two-well potential configuration. When they are diffusively coupled like in Eqs. (1), the stability of the resulting dynamical state can be studied through the linearization of these equations around the states  $x_k$  according to

$$\begin{aligned} \ddot{\xi}_k + \lambda \dot{\xi}_k + (1 + 3\gamma x_k^2) \xi_k &= K[\xi_{k+1} - 2\xi_k + \xi_{k-1}], \\ k &= 1, 2, 3, 4, \end{aligned} \tag{3}$$

where  $\xi_k$  stands for the perturbations. Each of these perturbations is parametrically excited by a chaotic variable  $x_k$ . The Fourier spectrum of the SWDO with  $\gamma > 0$  in the chaotic state shows that the energy is mainly distributed in very sharp bands around odd harmonics of  $\omega$ . But, the major part of the energy is around the fundamental mode, which is thus the most predominant. Consequently, we can in first approximation replace  $x_k$  in Eqs. (3) by

$$x_{\text{per}} = A_0 \cos(\omega t - \varphi), \tag{4}$$

where  $x_{\text{per}}$  is supposed to be the best uniperiodic approximation of  $x_k$ . The mathematical meaning of such a substitution is that the asymptotic behavior of each  $\xi_k$  will be decided by the optimized Floquet multipliers instead of the sub-Lyapunov exponents [12,13]. As reported in Refs. [12,13] dealing with the optimization of chaos synchronization, this first order approximation gives results in fairly good agreement with the numerical simulation.

If we introduce the diagonal variables (or Fourier modes)  $\zeta_s$  as

$$\begin{aligned} \zeta_1 &= \xi_1 + \xi_2 + \xi_3 + \xi_4, \\ \zeta_2 &= x_4 - x_2, \\ \zeta_3 &= x_3 - x_1, \\ \zeta_4 &= x_4 - x_3 + x_2 - x_1 \end{aligned} \tag{5}$$

and the following rescalings,

$$\begin{aligned} \tau &= \omega t, \\ \delta_0 &= \frac{1}{\omega^2} \left[ 1 + \frac{3}{2} \gamma A_0^2 - \frac{\lambda^2}{4} \right], \\ \alpha &= \frac{3\gamma A_0^2}{4\omega^2}, \\ \eta_s &= \zeta_s \exp\left[\frac{\lambda \tau}{2\omega}\right], \quad s = 1, 2, 3, 4, \end{aligned} \tag{6}$$

Eqs. (3) may now be written under the form of a set of independent canonical Mathieu equations, that is,

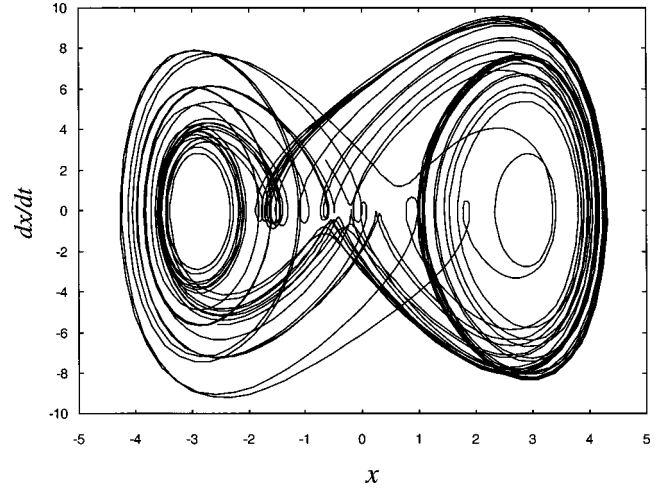


FIG. 1. Phase plane of the chaotic oscillator with  $\lambda=0.2$ ,  $\gamma=1.0$ ,  $\omega=0.86$ , and  $F=28.5$ .

$$\frac{d^2 \eta_s}{d\tau^2} + [\delta_s + 2\alpha \cos(2\tau - 2\varphi)] \eta_s = 0, \quad s = 1, 2, 3, 4, \tag{7}$$

with

$$\begin{aligned} \delta_1 &= \delta_0, \\ \delta_2 &= \delta_3 = \delta_0 + \frac{2K}{\omega^2}, \\ \delta_4 &= \delta_0 + \frac{4K}{\omega^2}. \end{aligned} \tag{8}$$

Floquet theory states that depending on  $\delta_s$  and  $\alpha$ ,  $\eta_s$  may either indefinitely grow to infinity or decay to zero, and thereby unambiguously decide the asymptotic behavior of the independent Fourier modes  $\zeta_s$  [13]. Consequently, the stability of each  $\zeta_s$  relies on the position of the representative point  $M_s(\delta_s, \alpha)$  on a stability map which is sometimes referred to as the Strutt diagram.

In Fig. 2, we have represented the Strutt diagram which is divided into three areas in the parametric plane  $(\delta, \alpha)$  [13]. The first of them is the area of linear stability where  $|\zeta(+\infty)| \rightarrow 0$ . It is the inner shaded zone of Fig. 2, and its boundaries can be either  $\pi$  periodic [ $\zeta(t) = \zeta(t + \pi/\omega)$ ] or  $2\pi$  periodic [ $\zeta(t) = \zeta(t + 2\pi/\omega)$ ]. The second zone is the area of instability where any perturbation diverges to infinity, i.e.,  $|\zeta(+\infty)| \rightarrow +\infty$ . This area is in blank in the Strutt diagram. At last, there is a buffer zone of nonlinear stability between the linearly stable and unstable areas, where  $0 < |\zeta(+\infty)| < +\infty$ . This latter zone (which is, however, linearly unstable) has been lightly shaded and cannot be predicted from the conventional Floquet analysis, since it originates from the nonlinear variational terms we have discarded in Eqs. (3).

We can now analyze through the Strutt diagram what happens in the system when the coupling strength  $K$  is continuously increased from zero to infinity. When  $K=0$ , the system is uncoupled and the Fourier modes  $\zeta_2$ ,  $\zeta_3$ , and  $\zeta_4$  degener-

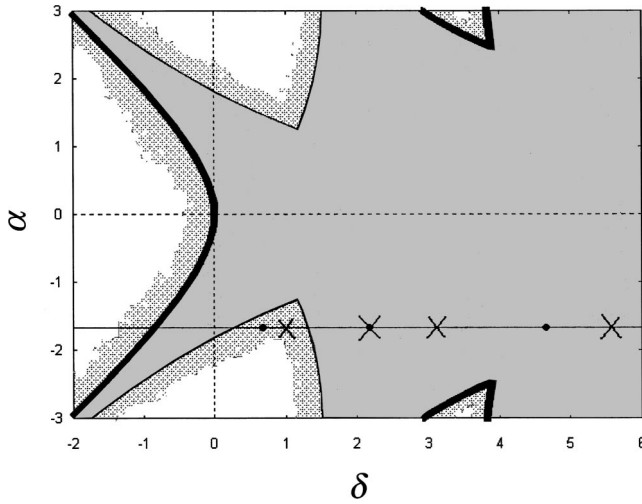


FIG. 2. The Strutt diagram. The  $\pi$ -periodic boundaries are represented by thick lines, and the  $2\pi$ -periodic boundaries are represented by thin lines. The nondegenerated spatial Fourier modes have been represented for  $G=0$  (points) and for  $G \neq 0$  (crosses).

ate into  $\zeta_1$ . Therefore, the whole system is represented by a single point  $M_0$  of coordinates  $(\delta_0, \alpha)$  in the Strutt diagram. It should be noticed that  $M_0$  automatically belongs to the nonlinear stability area since the uncoupled system is chaotic. As  $K$  is increased, the modes  $\zeta_2$ ,  $\zeta_3$ , and  $\zeta_4$  represented in the stability map by the related points  $M_s$  of coordinates  $(\delta_s, \alpha)$  independently begin to move from left to right along the straight horizontal line of equation  $\alpha = \text{const}$  with a “velocity”

$$v_s = \frac{d\delta_s}{dK}. \quad (9)$$

It results that  $\zeta_4$  is the fastest mode with a velocity  $v_4 = 4/\omega^2$ , while the degenerated modes  $\zeta_2$  and  $\zeta_3$  are the slowest with  $v_2 = v_3 = 2/\omega^2$ . These “mobile” modes are called transverse modes because they decide the stability of perturbations transverse to the complete synchronization manifold. On the other hand,  $\zeta_1$  remains immobile in the Strutt diagram since  $v_1 = 0$ : it is the longitudinal mode describing the stability along the synchronization manifold. When  $K$  is small, the three transverse mode points  $M_2$ ,  $M_3$ , and  $M_4$  remain in the vicinity of  $M_0$ , i.e., in the nonlinear stability zone. Therefore, the corresponding  $\zeta$  perturbations have a nonzero finite time-average value: we are in the regime of spatiotemporal chaos.

When the fastest mode  $\zeta_4$  reaches first the linearly stable area, the ring satisfies the constraint

$$x_4 - x_3 + x_2 - x_1 \equiv 0, \quad (10)$$

while we still have

$$\begin{aligned} x_1 &\neq x_3, \\ x_2 &\neq x_4, \end{aligned} \quad (11)$$

since  $\zeta_2$  and  $\zeta_3$  remain in the nonlinear stability buffer zone. The ring is therefore in a standard correlated state (SCS). This intermediate state differs from spatiotemporal chaos because of the constraint (10), and also from complete synchronization because of Eqs. (11).

If, on the other hand,  $M_4$  reenters into the buffer zone while  $M_2$  and  $M_3$  have yet together penetrated into the linearly stable area, we have

$$\begin{aligned} x_1 &\equiv x_3, \\ x_2 &\equiv x_4, \end{aligned} \quad (12)$$

and

$$x_4 - x_3 + x_2 - x_1 \neq 0. \quad (13)$$

This is sometimes referred to as cluster synchronization. Here, two clusters have emerged [Eqs. (12)] while there is no synchronization between these two clusters [Eqs. (13)].

At last, when the three transverse mode points  $M_2$ ,  $M_3$ , and  $M_4$  are together in the linearly stable area, the ring is in the complete synchronization state

$$x_4 = x_3 = x_2 = x_1, \quad (14)$$

corresponding to the simultaneous fulfillment of both Eqs. (10) and (12). In that case, all the oscillators display the same dynamics.

Numerical simulations confirm the bifurcation mechanism deduced from the Strutt diagram analysis. Let us consider the following two functions of the state variables:

$$g_4 = \langle |x_4 - x_3 + x_2 - x_1| \rangle, \quad (15)$$

$$g_{23} = \langle |x_4 - x_2| + |x_3 - x_1| \rangle, \quad (16)$$

where the brackets  $\langle \cdot \rangle$  stand for the time average.  $g_4$  represents  $\zeta_4$  on one hand, while  $g_{23}$  represents both  $\zeta_2$  and  $\zeta_3$  on the other. These functions will be equal to zero if the corresponding transverse modes points are in the linearly stable area of the Strutt diagram, and different from zero if they are in the buffer zone.

In Figs. 3(a) and 3(b), the variations of  $g_{23}$  and  $g_4$  are represented as a function of  $K$ . Effectively, for low  $K$  values, the ring is in the spatiotemporal chaos regime since  $g_{23} \neq 0$  and  $g_4 \neq 0$ . When  $K$  reaches 0.70,  $g_4$  first vanishes because the fastest mode point  $M_4$  enters the linear stability area: it is the standard correlated state. This is also witnessed when  $K$  is between 2.30 and 2.35 ( $g_{23} \neq 0$  and  $g_4 = 0$ ). On the other hand, when  $g_{23} = 0$  and  $g_4 \neq 0$ , like in the case  $1.05 < K < 1.20$ , we have a cluster synchronization state. At last, complete synchronization ( $g_{23} = g_4 = 0$ ) occurs between 1.20 and 1.70, and also when  $K > 2.35$ . It is important to notice that the transitions between these dynamical states are never sharp. Moreover, unstable invariant sets embedded within the chaotic attractor can perturb the stability of the Fourier modes, like for  $K \approx 1.00$  or  $K \approx 1.75$ .

The above stability analysis can be generalized to a wide range of chaotic  $N$ -oscillator coupled systems through the master stability function (MSF) technique [7]. Even though

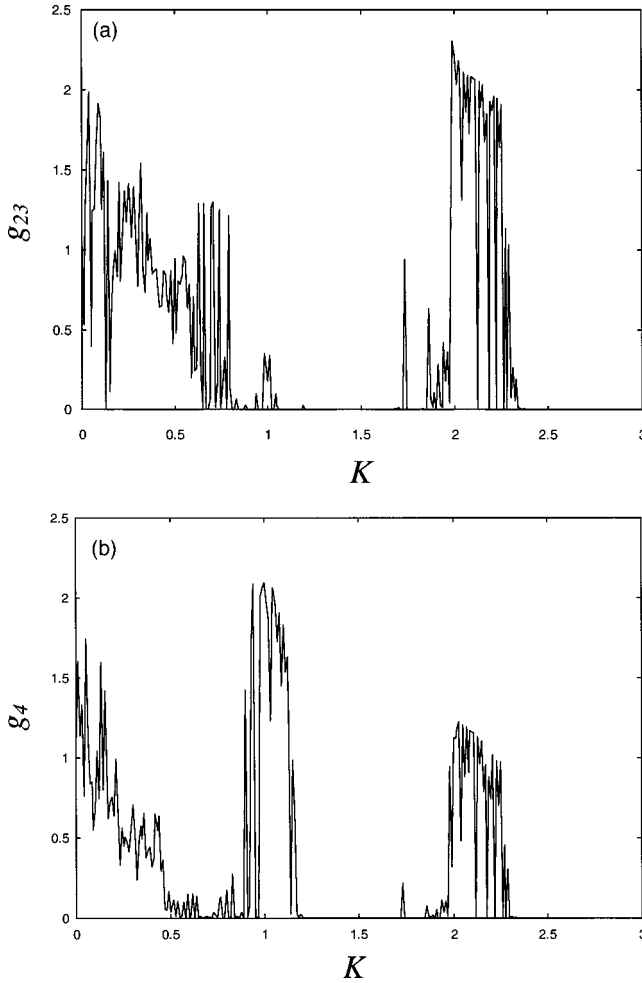


FIG. 3. (a) Variations of  $g_{23}$  as a function of  $K$ , (b) idem for  $g_4$ .

that method was originally developed to investigate the stability of the completely synchronous motion, it can, however, enable one to understand the various phenomena that have yet been numerically encountered in some coupled systems (intermittent pattern formation, symmetry breaking, spontaneous spatial reordering, etc.). Effectively, the MSF method enables one to decide the stability of the transverse modes, and therefore, the cluster and correlated states would also be interpreted as the dynamical configurations corresponding to the various distributions of these transverse modes between the linearly and nonlinearly stable areas of the related parameter space.

### III. INFLUENCE OF THE LOCAL INJECTION ( $G \neq 0$ )

When  $G$  is taken into account, the first order perturbation equations are

$$\ddot{\xi}_1 + \lambda \dot{\xi}_1 + (1 + 3\gamma\bar{x}_c^2)\xi_1 = K(\xi_4 - 2\xi_1 + \xi_2) - G\xi_1,$$

$$\ddot{\xi}_k + \lambda \dot{\xi}_k + (1 + 3\gamma\bar{x}_c^2)\xi_k = K(\xi_{k+1} - 2\xi_k + \xi_{k-1}), \quad k=2,3,4, \quad (17)$$

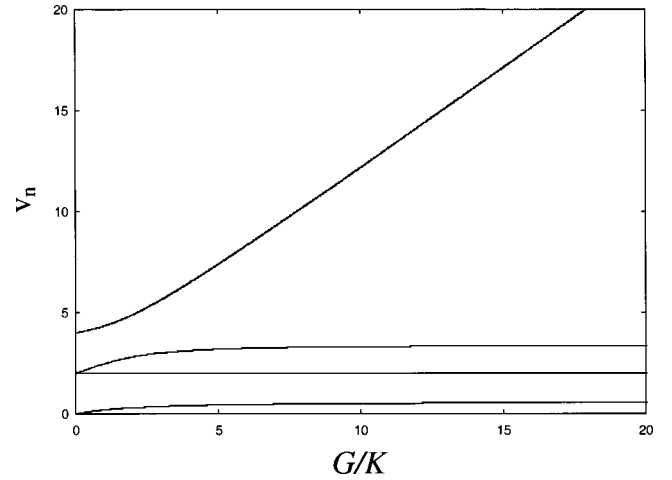


FIG. 4. Velocities (in units of  $1/\omega^2$ ) of the Fourier modes when the ratio ( $G/K$ ) is increased.

with  $\xi_k = x_k - \bar{x}_c$ . From these equations, we can determine the eigenvalues  $\Lambda_n$  through the resolution of the characteristic fourth-order polynomial equation,

$$\Gamma^4 + \left(\frac{G}{K}\right)\Gamma^3 - 4\Gamma^2 - 2\left(\frac{G}{K}\right)\Gamma = 0, \quad (18)$$

where the solutions  $\Gamma_n$  are related to the eigenvalues  $\Lambda_n$  and the velocities  $v_n$  by

$$\Gamma_n = 2 - \frac{\Lambda_n}{K} = 2 - \omega^2 v_n. \quad (19)$$

Figure 4 shows the numerical solutions of Eqs. (18) obtained with the Newton-Raphson algorithm when the ratio ( $G/K$ ) is increased. It can be noticed that when  $G=0$ , we have three nondegenerated modes, as we have demonstrated in the preceding section. But as soon as  $G \neq 0$ , the degeneracy of the second mode is destroyed so that four nondegenerated modes now appear, and the slowest one discontinuously passes from  $v_{2,3} = 2/\omega^2$  to  $v_1 = 0^+$ . Moreover, it appears that  $v_4$  indefinitely increases to infinity, while the second mode keeps a constant velocity  $v_2 = 2/\omega^2$ .

Each of these nondegenerated modes has been schematically represented in the Strutt diagram in Fig. 2 by crosses of coordinates  $(\delta_s, \alpha)$  with

$$\delta_1 = \delta_0 + \nu_1 K = \delta_0 + \frac{\varepsilon_1}{\omega^2} K,$$

$$\delta_2 = \delta_0 + \nu_2 K = \delta_0 + \frac{2}{\omega^2} K,$$

$$\delta_3 = \delta_0 + \nu_3 K = \delta_0 + \frac{2 + \varepsilon_3}{\omega^2} K,$$

$$\delta_4 = \delta_0 + \nu_4 K = \delta_0 + \frac{4 + \varepsilon_4}{\omega^2} K.$$

(20)

The  $\delta_s$  parameters have been explicitly written to define the detuning functions  $\varepsilon_s$  which are obviously equal to 0 when  $G=0$ . However,  $\nu_1$  and  $\nu_3$  asymptotically converge to the limit values  $\varepsilon_1^\infty/\omega^2$  with  $\varepsilon_1^\infty=0.585$  and  $(\varepsilon_3^\infty+2)/\omega^2$  with  $\varepsilon_3^\infty=1.414$ , respectively, when  $G\rightarrow+\infty$ .

**A. Generalized correlated states**

The determination of the dynamical state of the ring now depends on the distribution of the four nondegenerated Fourier modes between the various areas of the Strutt diagram. If we consider  $\mathbf{T}$  as the transfer matrix from the perturbation variables  $\xi_i$  to the diagonal ones  $\zeta_k$ , we have the following equations:

$$\zeta_k = \sum_{i=1}^4 T_{ik} \xi_i. \tag{21}$$

Here, the  $T_{ik}$  coefficients are complicated functions of  $G$  and  $K$  which can be obtained through an eigenvector analysis of Eqs. (17). They are, however, simply equal to 0, 1, or  $-1$  when  $G=0$ .

For very small  $K$  values, the mode points are still in the nonlinear buffer zone, so that the ring remains in the spatiotemporal chaos state. When  $K$  is increased, the fastest mode becomes linearly stable, i.e.,

$$\zeta_4 = \sum_{i=1}^4 T_{i4}(x_i - \bar{x}_c) = 0. \tag{22}$$

This latter equation expresses a nontrivial linear constraint between the four dynamical variables  $x_i$ : we consider this intermediate state as a generalized correlated state (GCS) by opposition to the SCS we have analyzed in Sec. II. Equation (22) means that knowing the  $\bar{x}_c$  command variable, each ring displacement  $x_j$  can be related to the three others as

$$x_j = \bar{x}_c + \sum_{\substack{i=1 \\ i \neq j}}^4 \frac{T_{i4}}{T_{j4}} (x_i - \bar{x}_c). \tag{23}$$

This may have a conceptual application to the enhancement of the chaotic encryption of messages [4]. Effectively, in the classical scheme, only two chaotic oscillators are synchronized. Hence, one can encode an information-bearing signal into the noiselike output of the chaotic transmitter while the synchronous receiver identifies the masking component which is then extracted to reveal the original transmitted message.

In the four-oscillator ring with a local injection, security is strengthened when the encryption is performed with the  $x_j$  variable rather than with  $\bar{x}_c$ . Effectively, according to Eq. (23), it is indispensable in that case to know the dynamics of the three other chaotic oscillators to recover the encoded message. Therefore, one can consider that these three complementary oscillators enable the chaotic component to be more complex, i.e., more difficult to pirate. When a second nondegenerated mode becomes linearly stable, a supplementary constraint is imposed so that each chaotic oscillator

of the ring can be univocally related to only two others. In this case, obviously, the masking component is less complex. If a third mode also becomes stable, each oscillator will be related to a single other one and at last, complete chaotic synchronization with the external master oscillator occurs when the four modes become linearly stable. This latter case corresponds to the classic masking technique, since the four-oscillator ring is now equivalent to a single oscillator. Obviously, the above reasoning can also be extended to the  $N$ -oscillator system.

**B. Transition boundary values for generalized clusters states**

The transition boundaries between the spatiotemporal chaos, GCS, and complete synchronization states are mainly influenced by both  $G$  and  $K$ . Let us, for example, focus on the first bifurcation (from spatiotemporal chaos to GCS) and on the last one (from GCS to complete synchronization) as  $K$  is increased with a fixed  $G$ . The corresponding critical transition values for  $G=0$  have yet been determined numerically in Sec. II as  $K_f(0)=0.70$  and  $K_l(0)=2.35$ . They can be used to deduce analytically the transition values  $K_f(G)$  and  $K_l(G)$  for any nonzero  $G$  value. Note that for  $G \neq 0$  we should have spatiotemporal chaos for  $K < K_f(G)$ , complete synchronization for  $K > K_l(G)$ , and GCS when  $K_f(G) \leq K \leq K_l(G)$ .

In fact, the first GCS emerges when the fastest mode point  $M_4$  enters the linear stability area of the Strutt diagram. From Eqs. (8), (9), and (20), we can therefore deduce that

$$\int_{\delta_0}^{\delta_{cr,f}} d\delta = \int_0^{K_f(0)} \frac{4}{\omega^2} dK = \int_{0^+}^{K_f(G)} \frac{1}{\omega^2} \left[ 4 + \varepsilon_4 \left( \frac{G}{K} \right) \right] dK, \tag{24}$$

i.e.,

$$\int_{0^+}^{K_f(G)} \varepsilon_4 \left( \frac{G}{K} \right) dK = 4[K_f(0) - K_f(G)], \tag{25}$$

where  $\delta_{cr,f}$  is the first critical Hopf boundary value encountered as  $\delta$  is increased. Since the integrand function  $\varepsilon_4$  is positive, one can straightforwardly deduce that

$$K_f(G) \leq K_f(0). \tag{26}$$

Hence, the ring emerges more rapidly from spatiotemporal chaos when  $G$  is greater. However,  $K_f(G)$  cannot be expressed explicitly because  $\varepsilon_4$  has not been determined analytically.

On the other hand, the boundary transition from the last GCS to the complete chaotic synchronization state corresponds to the entrance of the slowest mode point  $M_1$  into the last semi-infinite linear stability section, so that we have

$$\int_{\delta_0}^{\delta_{cr,f}} d\delta = \int_0^{K_f(0)} \frac{2}{\omega^2} dK = \int_{0^+}^{K_f(G)} \frac{1}{\omega^2} \varepsilon_1 \left( \frac{G}{K} \right) dK, \tag{27}$$

i.e.,

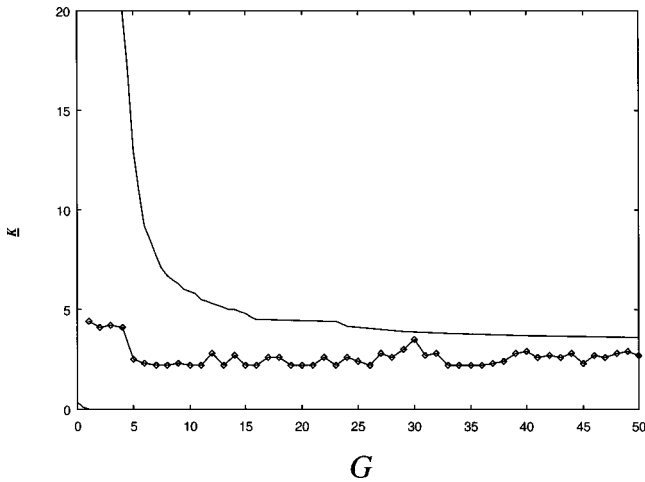


FIG. 5. Transition boundaries from GCS to complete synchronization. The analytical results are shown by full line, and the numerical results are shown by squares linked by a continuous line.

$$\int_{0^+}^{K_l(G)} \varepsilon_1 \left( \frac{G}{K} \right) dK = 2K_l(0). \quad (28)$$

Here,  $\delta_{cr,f}$  is the last critical Hopf boundary value. Therefore,  $K_l(G)$  converges to the asymptotic value

$$K_l(G \rightarrow +\infty) \approx \frac{2}{\varepsilon_1} K_l(0) > K_l(0). \quad (29)$$

The above equation means that as  $K$  is increased, complete synchronization paradoxically occurs later when a local injection coupling is introduced. It can consequently be considered that the related gap energy is used to tune the synchronous chaotic ring to the target master oscillator.

The critical boundary curves  $K_f(G)$  and  $K_l(G)$  have been plotted in Fig. 5. They divide the parametric plane into three

areas: the lower zone corresponds to spatiotemporal chaos, the intermediate one to the GCS, and the uppermost to the complete synchronization. However, the curve  $K_f(G)$  remains difficult to distinguish in the figure, since it rapidly vanishes to 0. Therefore, the lower zone of spatiotemporal chaos does not clearly appear on the map. On the same figure, the results of the numerical simulation for  $K_l(G)$  have also been represented. They show a qualitative concordance with the analytic results of Eq. (28). One can note the discontinuity at  $G=0$  for the  $K_l(G)$  curve, due to the drop to  $0^+$  of the slowest velocity when the local injection is set on. This implies that small  $G$  values (case corresponding to undesirable external perturbations) irreversibly destroy the complete synchronization state since the threshold value jumps from a finite value to infinity. However, it appears that the boundary curves rapidly converge to their asymptotes, so that it is not necessary to use high  $G$  values to obtain a satisfying synchronization.

#### IV. CONCLUSION

In summary, we have studied the dynamics and bifurcation behavior of a ring of chaotic oscillators with a local injection. Floquet theory has enabled to interpret through the Strutt diagram the various transitions amongst the different dynamical states of the system. The influence of local injection has also been investigated, and a particular emphasis has been laid upon the generalized correlated states. The boundaries from these GCS to spatiotemporal chaos and complete synchronization have been derived.

The extension of our approach to the thermodynamic limit ( $N \rightarrow +\infty$ ) and to the continuous media approximation seems to be an important perspective. This study may also shed some light on various interesting issues such as the collective behavior of small aggregates of coupled cells in biology [5], or the problem of interconnection in chaos-secured communication networks.

- 
- [1] D. K. Umbarger, C. Grebogi, E. Ott, and B. Afeyan, Phys. Rev. A **39**, 4835 (1989).
  - [2] J. F. Heagy, T. L. Carroll, and L. M. Pecora, Phys. Rev. E **50**, 1874 (1994).
  - [3] J. F. Heagy, T. L. Carroll, and L. M. Pecora, Phys. Rev. Lett. **74**, 4185 (1995).
  - [4] K. M. Cuomo and A. V. Oppenheim, Phys. Rev. Lett. **71**, 65 (1993); P. Woaf0, Phys. Lett. A **267**, 31 (2000).
  - [5] V. N. Belykh, I. V. Belykh, and E. Mosekilde, Phys. Rev. E **63**, 036216 (2001).
  - [6] S. E. de S. Pinto, S. R. Lopes, and R. L. Viana, Physica A **303**, 339 (2002).
  - [7] K. S. Fink, G. Johnson, T. Carroll, D. Mar, and L. Pecora, Phys. Rev. E **61**, 5080 (2000).
  - [8] M. Zhan, G. Hu, and J. Yang, Phys. Rev. E **62**, 2963 (2000).
  - [9] Y. Zhang, G. Hu, H. A. Cerdeira, S. Chen, T. Braun, and Y. Yao, Phys. Rev. E **63**, 026211 (2001).
  - [10] Y. Zhang, G. Hu, and H. A. Cerdeira, Phys. Rev. E **64**, 037203 (2001).
  - [11] G. Hu, J. Xiao, J. Gao, X. Li, Y. Yao, and H. Bambi, Phys. Rev. E **62**, R3043 (2000).
  - [12] P. Woaf0 and R. A. Kraenkel, Phys. Rev. E **65**, 036225 (2002).
  - [13] Y. Chembo Kouomou and P. Woaf0, Phys. Lett. A **298**, 18 (2002).